ACS Partner Journal

CHEMICAL & BIOMEDICAL IMAGING

pubs.acs.org/ChemBioImaging

Article

Distinguishing Single-Metal Nanoparticles with Subdiffraction Spatial Resolution Using Variable-Polarization Fourier Transform Nonlinear Optical Microscopy

Megan A. Steves and Kenneth L. Knappenberger, Jr.*

Cite This: *Chem. Biomed. Imaging* 2023, 1, 91−98

Read Online

ACCESS | Metrics & More | Article Recommendations | Supporting Information

ABSTRACT: The development and use of interferometric variable-polarization Fourier transform nonlinear optical (vpFT-NLO) imaging to distinguish colloidal nanoparticles colocated within the optical diffraction limit is described. Using a collinear train of phase-stabilized pulse pairs with orthogonal electric field vectors, the polarization of nonlinear excitation fields are controllably modulated between linear, circular, and various elliptical states. Polarization modulation is achieved by precise control over the time delay separating the orthogonal pulse pairs to within hundreds of attoseconds. The resultant emission from gold nanorods is imaged to a 2D array detector and correlated to the excitation field polarization and plasmon resonance frequency by Fourier transformation. Gold nanorods with length-to-diameter aspect ratios of 2 support a longitudinal surface plasmon resonance at approximately 800 nm, which is resonant with the excitation fundamental carrier wavelength. Differences in the intrinsic linear and circular dichroism resulting from variation in their relative alignment with respect to the laboratory frame enable optical differentiation of nanorods separated within 50 nm, which is an approximate 5-fold improvement over the diffraction limit of the microscope. The experimental results are supported by analytical simulations. In addition to subdiffraction spatial resolution, the vpFT-NLO method intrinsically provides the polarization- and frequency-dependent resonance response of the nanoparticles—providing spectroscopic information content along with super-resolution imaging capabilities.

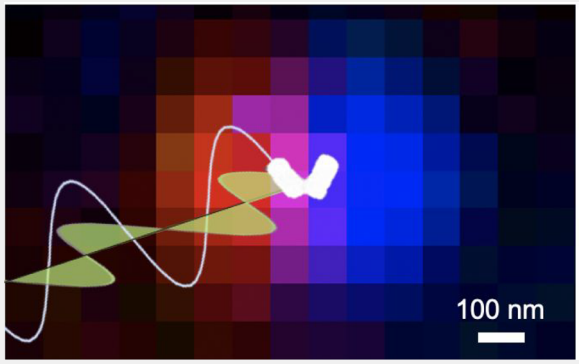

KEYWORDS: *nonlinear optics, polarization, circular dichroism imaging, Fourier transform spectroscopy, plasmons, super-resolution microscopy*

INTRODUCTION

The observation of emission from individual molecules or particles can reveal subpopulations among the manifold of heterogeneous states that are often obscured in ensemble measurements.[1,2] Single-molecule detection has also been foundational for super-resolution imaging through single-molecule localization microscopy (SMLM). Conventional diffraction-limited single-molecule images are generated by projecting emission photons to a two-dimensional array. Owing to light diffraction, the emission image is distributed as a 2D Gaussian with dimensions significantly larger than typical molecular diameters and approximated as half the emission wavelength. SMLM methods overcome the mismatch between point source and PSF dimensions through statistical positional localization of the emitter. In essence, SMLM reduces the uncertainty associated with the center of the 2D Gaussian representing the PSF so that the emission source can be spatially pinpointed. SMLM techniques have become ubiquitous in visualizing heterogeneous dynamics, structure, and various other properties of biological and materials systems. Recently, multidimensional super-resolution techniques have emerged,[3] which can enrich the information content of optical images with additional spectroscopic, temporal, and polarization observables.[4−7]

Expansion of the spatial point spread function into one or more additional dimensions allows super-resolution microscopy methods based on single-molecule localization to distinguish molecules that are unresolvable when only spatial dimensions are used.[8,9] In common single-molecule localization microscopy techniques[10−13] the added dimension is temporal, as the emission from molecules with spatially overlapping point spread functions (PSFs) is stochastically separated in time, allowing specific point source positions to be determined individually. However, spectral or polarization

Received: January 9, 2023
Revised: February 9, 2023
Accepted: February 14, 2023
Published: March 6, 2023

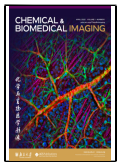

https://doi.org/10.1021/cbmi.3c00008
Chem. Biomed. Imaging 2023, 1, 91−98

dimensions could also be used to separate emitters which are spatially colocated within the diffraction limit. Polarization-modulation in combination with deconvolution and reconstruction algorithms has previously been used as an avenue to achieving subdiffraction spatial resolution, as well as information about emission dipole orientation.[14−16] In these cases, the polarization-response is specific to the emission, typically fluorescence, signals. However, the excitation resonance response—both spectrally and polarization resolved—of an object is informative in many aspects and therefore desirable to obtain. Polarization-resolved SHG microscopy has been used to study single plasmonic nanostructures[17] with subdiffraction spatial resolution[18] but does not provide complementary information about the spectral resonance response. Photothermal circular dichroism (CD) microscopy provides single-particle sensitivity using lock-in detection but is not compatible with subdiffraction spatial resolution.[19,20] Here, we demonstrate that single nanoparticles can be separated and localized based on their polarization response along with simultaneous resolution of their spectra.

Alongside multidimensionality, recent progress in super-resolution microscopy has emphasized label-free methods to avoid perturbation of the sample and overcome issues of photobleaching.[21] Nonlinear optical microscopy is an ideal platform for label-free, multidimensional super-resolution microscopy, as it provides contrast through the structural and chemical specificity of various nonlinear optical signals, without the need for fluorescent labels.[22,23] Our previous work has demonstrated that Fourier transform spectroscopy can be used to distinguish particles with subdiffraction spatial resolution based on their spectroscopic response.[24] In Fourier transform nonlinear optical (FT-NLO) microscopy, the intrinsic nonlinear optical response of a particle, such as harmonic generation or multiphoton photoluminescence (MPPL), is modulated based on the particle resonance, allowing subdiffraction spatial resolution while retaining spectroscopic information. Unlike other SMLM methods, the temporal modulation is nonstochastic and reports on the excitation spectrum of an individual particle. However, as it relies on the spectral heterogeneity of the emitters, this method is limited to cases when neighboring emitters have sufficiently distinct resonance responses.

In this work, we expand spectrally determined FT-NLO super-resolution microscopy to address this limitation through the addition of a dimension corresponding to the polarization dependence of the emission. Variable polarization (vp) FT-NLO microscopy encodes the frequency- and polarization-dependent emission from a nonlinear-active sample, allowing emitters to be distinguished based on both their spectra and responses to different excitation polarization states. Here, we apply vpFT-NLO microscopy to plasmonic gold nanorods, taking advantage of differences between resonance responses of individual particles imparted by their intrinsic structural heterogeneity. The gold nanorods studied in this work have a longitudinal surface plasmon resonance (LSPR) resonant with the broadband laser fundamental centered at 1.55 eV (Figure S1). However, variations in the nanorod's aspect ratio, among other factors, can red-shift or blue-shift the LSPR of an individual rod with respect to the mean ensemble plasmon resonance frequency.[25] Resonant enhancement of the nonlinear signal by the LSPR also affects the polarization-dependent response, as the LSPR is only efficiently excited by electric fields parallel to the long axis of the nanorod, resulting in a strong linear dichroism. Chiroptical nonlinear responses have also been observed in individual gold nanorods in association with the LSPR, arising from small asymmetries in the nanorod structure.[26] Thus, subtle structural variations among nanorods are expected to produce distinct frequency- and polarization-dependent nonlinear optical responses. Although we demonstrate the ability to distinguish gold nanorods with subdiffraction spatial resolution using vpFT-NLO microscopy, the technique described in this work should be applicable for separating any nano-objects with distinct polarization- or frequency-dependent nonlinear responses. The vpFT-NLO microscopy technique described here can provide subdiffraction localization of emitters without the need for labeling, as in many conventional super-resolution techniques, while also providing information about the frequency- and polarization-dependent response that is not obtained in other methods.

EXPERIMENTAL METHODS AND THEORETICAL BACKGROUND

In vpFT-NLO microscopy, the polarization of the excitation beam is continuously varied using a pulse replica generator which has been described previously. A translating-wedge-based identical pulses encoding system (TWINS)[27] controls the polarization state of light through the Babinet-Soleil effect by altering the relative phase between x- and y-polarized components of the electric field.[28] The pulse delay generator (Figure 1a) consists of a series of birefringent optics which split an incident parent pulse into two phase-stable replicas with a controllable interpulse delay time, τ. A polarizer is first used to orient the parent pulse polarization at 45° with respect to both the ordinary E_x and extraordinary E_y axis of the nonlinear crystals. The E_x direction will be referred to as the

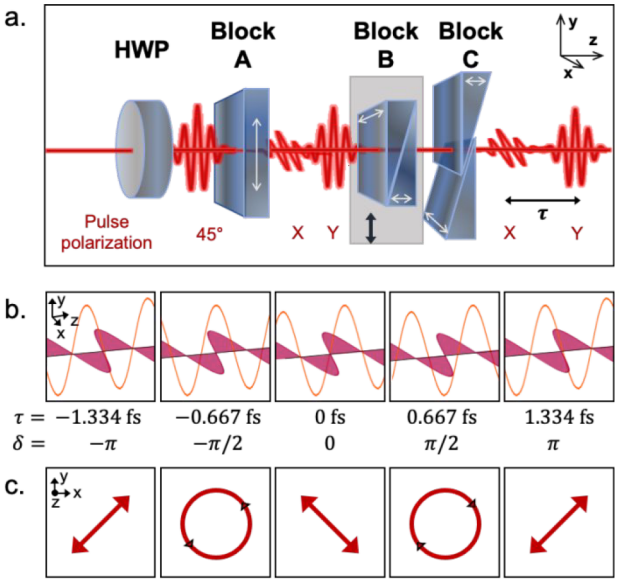

Figure 1. Generation of variable polarization states in vpFT-NLO microscopy. (a) TWINS pulse delay generator consisting of a half-wave plate (HWP) and three α-BBO blocks which split the parent pulse into its x- and y-polarized components and controls the time delay between them, as described in the text. (b) Example time delays and corresponding phase shifts for an 800 nm excitation pulse, which produce the linear and circular polarization states shown in (c).

https://doi.org/10.1021/cbmi.3c00008
Chem. Biomed. Imaging 2023, 1, 91−98

laboratory frame hereafter, and will be used as the point of reference for depicting excitation field polarization states. The first nonlinear crystal, block A, converts the parent pulse into two orthogonally polarized pulses with a fixed interpulse time delay τ. Blocks B and C are used to adjust the interpulse time delay of the orthogonal pulse pair on the attosecond to femtosecond times scale. Previous research from our group has shown the ability to hold τ values of smaller than 12 as for 2 h, which is more than sufficient for the polarization-dependent measurements described here. Figure 1b,c contains a schematic illustrating how the polarization state of a monochromatic beam with carrier frequency ω_0 can be controlled by tuning τ. The polarization state for light propagation in the z-direction can be described with a Jones formalism:

$$E(t) = \begin{pmatrix} E_{0x}e^{i\phi_x} \\ E_{0y}e^{i\phi_y} \\ 0 \end{pmatrix} e^{i(kz-\omega_0 t)} \tag{1}$$

where $E(t)$ is the time-dependent electric field, E_{0x} and E_{0y} are the amplitudes of the x- and y-electric field components, respectively, with phases ϕ_x and ϕ_y, and k is the wavevector. Neglecting the zero E_z term, setting $\phi_x = 0$, and defining the relative phase difference $\delta = \phi_x - \phi_y$, eq 1 becomes

$$E(t, \tau) = \begin{pmatrix} E_0 \\ E_0 e^{i\delta} \end{pmatrix} e^{-i\omega_0 t} = \begin{pmatrix} E_0 \\ E_0 e^{i(\tau/\omega_0)} \end{pmatrix} e^{i(kz-\omega_0 t)} \tag{2}$$

where $E_0 = E_{0x} = E_{0y}$. With a zero interpulse time delay, the x- and y-polarization components will add to generate a pulse polarized at 45° with respect to the laboratory frame. When τ corresponds to a $\pi/2$ phase shift with respect to the carrier wave (e.g., τ = 670 as for 800 nm light), the fundamental will be circularly polarized. To generate the opposite handedness of circularly polarized light, a $-\pi/2$ phase shift (τ = −670 as) is introduced. A τ value corresponding to a $\pm\pi$ phase shift (τ = ±1.33 fs) will generate an excitation source polarized at ±45° with respect to the laboratory frame. Other values of τ corresponding to phase shifts between $-\pi$ and π will generate various degrees of elliptically polarized light.[28]

In order to demonstrate how vpFT-NLO microscopy can be used for super-resolution microscopy, we first develop a formalism to describe the interferometic nonlinear optical signal from a nanoparticle excited with various polarizations. In this work, the nanorod longitudinal surface plasmon resonance (LSPR) mode is resonant with the fundamental. The interaction with a resonant excitation pulse pair generates a plasmon field, $E_{pl}(t,\tau)$, which is the dominant driver of the nonlinear emission signal. The emitted nonlinear signal is collected as τ is controllably incremented. The n-th order nonlinear emission signal is expressed as

$$S^{(n)}(\tau) = \left| \int_{-\infty}^{\infty} (E_{pl}(t, \tau))^n dt \right|^2 \tag{3}$$

In the following, we assume a second order nonlinear signal (n = 2). The plasmon field itself is driven by the electric field of the pulse pair. For broadband pulses, the electric field vector of the pulse pair as a function of τ where the x-polarized component is treated as stationary is given by

$$E(t, \tau) = \begin{pmatrix} E_x \\ E_y \end{pmatrix} = \begin{pmatrix} E_0(t) \\ E_0(t-\tau) \end{pmatrix} \tag{4}$$

where the field of a single pulse, $E_0(t)$, is

$$E_0(t) = A_0 e^{-i\omega_0 t} \tag{5}$$

The excitation of the plasmon by polarized light described by the complex vector above can be modeled using a 2 × 2 Jones matrix, T. The plasmon field driven by the excitation pulse pair is

$$E_{pl}(t, \tau) = \begin{pmatrix} E_{pl,x}(t, \tau) \\ E_{pl,y}(t, \tau) \end{pmatrix} \propto \int_0^t e^{-i\omega_{pl}(t-t')\gamma/2} \begin{pmatrix} T_{11} & T_{12} \\ T_{21} & T_{22} \end{pmatrix} \begin{pmatrix} E_x(t') \\ E_y(t'-\tau) \end{pmatrix} dt' \tag{6}$$

where ω_{pl} is the plasmon resonance frequency and γ is the plasmon homogeneous line width, which are treated as independent of the excitation polarization.

Using the generalized matrix equivalence theorem,[29] the Jones transfer matrix describing the interaction of the plasmon mode with polarized light, T^{gen}, can be written as a combination of elements related to the physical parameters of the system:

$$T^{gen} = T^{CP}T^{LP}T^{CA}T^{LA} \tag{7}$$

The matrix T^{CP} (T^{LP}) describes circular (linear) birefringence of the sample, while linear and circular dichroism are described by T^{CA} and T^{LA}, respectively. In this study, we neglect birefringence to focus on the dichroic properties of the sample. Circular dichroism, or circular amplitude anisotropy, has the Jones matrix

$$T^{CA} = \begin{pmatrix} 1 & -iR \\ iR & 1 \end{pmatrix} \tag{8}$$

where R is the difference in absorption of left and right circularly polarized fields. Similarly, linear dichroism has the Jones matrix

$$T^{LA} = \begin{pmatrix} \cos^2\theta + P\sin^2\theta & (1-P)\cos\theta\sin\theta \\ (1-P)\cos\theta\sin\theta & \sin^2\theta + P\cos^2\theta \end{pmatrix} \tag{9}$$

where P is the difference in absorption of linear orthogonally polarized fields and θ is the angle of the major axis with respect to the lab frame. Multiplication of T^{CA} and T^{LA} gives the generalized transfer matrix for the nanorod with a given combination of linear and circular dichroism. For gold nanorods, linear dichroism is expected to be the main contributor as the plasmon absorption at the fundamental is greatest when the polarization of the exciting field is aligned with the long axis of the rod, corresponding to the longitudinal plasmon mode. However, circular dichroism in second harmonic generation, possibly reflecting asymmetric structure around the tips of the nanorods, has also been reported.[26]

With this formalism, we can predict the effects of linear and circular dichroism on the nonlinear interferometric signal measured in vpFT-NLO (Figure 2). The effects of linear dichroism are discussed first. Figure 2a shows the predicted response for a hypothetical particle with a plasmon resonance

https://doi.org/10.1021/cbmi.3c00008
Chem. Biomed. Imaging 2023, 1, 91−98

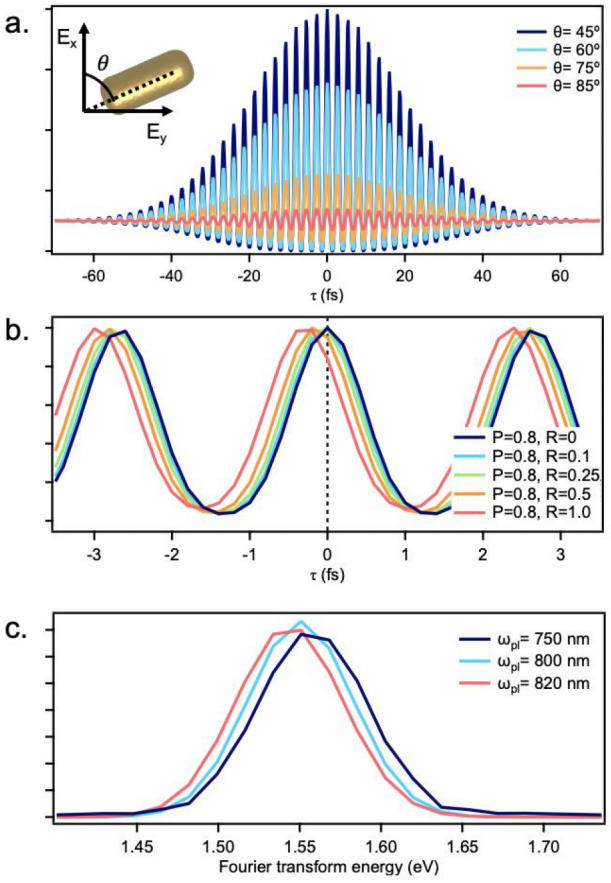

Figure 2. Modeling the effects of particle parameters on vpFT-NLO interferogram. (a) Rotating the angle of the nanorod longitudinal axis (θ) with respect to the lab frame (E_x) from 45 to 85° causes a decrease in the amplitude of the interferogram for a particle with P = 1 and R = 0. (b) Increasing the amount of circular dichroism, R, for a nanoparticle with a fixed θ value of 75° and P = 0.8 results in changes to the phase and amplitude of the interferogram. (c) Changes to the plasmon resonance frequency result in shifts of the spectrum obtained by Fourier transformation of the vpFT-NLO interferogram.

at 800 nm and a linear differential absorption, P, of 1. As the in-plane angle, θ, of the nanorod longitudinal axis changes (increases) with respect to the laboratory frame (E_x), the amplitude of the interference decreases. However, the normalized Fourier transform spectrum at the fundamental frequency does not change (Figure S2). At θ = 0 or 90° (not shown), the response from the particle is constant with respect to the interpulse time delay. Next, we examine the effect of an arbitrary amount of circular dichroism on the nonlinear interferogram. Figure 2b shows the response of a particle at θ = 75°, with a constant P of 0.8. The P value is reduced from 1 in order to permit circular dichroism effects, but kept significant to reasonably correspond to the nanorod system considered here. As the circular dichroism characterized by R increases, the phase of the interferogram shifts. For a particle with pure circular and no linear dichroism, we expect a phase shift of $\pm\pi/2$. When both linear and circular dichroism are present, as expected for the gold nanorods studied here, intermediate phase shifts are observed which are also dependent on the angle of the nanorod axis. Minor changes to the amplitude of the interferogram are also observed as R increases. Finally, we observe the effect of changes to the plasmon frequency in Figure 2c. As in FT-NLO, the variable polarization Fourier transform spectrum responds to spectral shifts in the plasmon resonance. Heterogeneity in the plasmon frequency of the nanorods studied in this work can be used to distinguish particles in super-resolution imaging applications, as discussed later.

From the above discussion, we can draw several qualitative conclusions about the appearance of interferometric signal from a nanoparticle with linear and circular dichroism, which help demonstrate the potential use of vpFT-NLO microscopy for subdiffraction limited microscopy:

1. In the absence of circular dichroism, and a large constant linear dichroism, the nanorod behaves much like a polarizer used in traditional FT-NLO or interferometric autocorrelations. For θ = 45°, an 8:1 ratio between the signal at τ = 0 and the signal at long time delays is obtained. This is expected based on the equation for an n-order interferometric autocorrelation

$$\mathrm{IAC}^{(n)}(\tau) = \int_{-\infty}^{\infty} |\{E(t) + E(t+\tau)\}^n|^2 \mathrm{d}t \tag{10}$$

which predicts a ratio $\frac{\mathrm{IAC}^{(n)}(0)}{\mathrm{IAC}^{(n)}(\infty)}$ of 2^{2n-1}.[30] For other values of θ, the modulation of the signal with polarization decreases.

2. In the presence of a large but <1 linear differential absorption, circular dichroism manifests as a shift in the phase of the interferogram as well as a change in the modulation amplitude. The magnitude of the phase shift is dependent on the relative contribution of circular and linear dichroism in the measurement.

3. In all cases, the frequency and line width of the fundamental peak in the spectrum in vpFT-NLO reflects the characteristics of the plasmon resonance. Therefore, similarly to FT-NLO, the plasmon response function in the frequency domain can be extracted using

$$S^{(n)}(\omega) = |R^{(1)}(\omega)E(\omega)|^2 \tag{11}$$

where $S^{(n)}(\omega)$ is the signal near ω_0, $R^{(1)}(\omega)$ is the linear response function, and $E(\omega)$ is the electric field of the fundamental laser.

Based on the above, we conclude that a single nanoparticle's polarization response and plasmon response function will affect the phase, amplitude, and frequency of the vpFT-NLO spectrum and may be used as additional axes for detecting nanoparticles which are spatially colocated in the diffraction limit. Hence, inspection of NLO interferograms provide rich details about the sample nonlinear optical response that would not be attainable from conventional, steady-state measurements. We note that vpFT-NLO provides two new observables beyond the FT-NLO method. First, the amplitude of the modulation at ω_0 varies with the angle of the nanorod and the degree of dichroism. The modulation is characterized by the contrast ratio $\frac{s^{(n)}_{t=0}}{s^{(n)}_{t=\infty}}$, which is restricted to 8:1 for a second-order FT-NLO measurement. In vpFT-NLO, however, the contrast ratio can have values of $1 \leq \frac{s^{(n)}_{t=0}}{s^{(n)}_{t=\infty}} \leq 2^{2n-1}$, where n is the photon order of the nonlinear signal. Second, the phase of the vpFT-NLO interferogram can be shifted by circular dichroism, whereas the phase is fixed in other Fourier transform spectroscopies, allowing samples with circular dichroism to be distinguished from purely achiral samples. While quantitative extraction of linear and circular dichroism

https://doi.org/10.1021/cbmi.3c00008
Chem. Biomed. Imaging 2023, 1, 91−98

parameters from vpFT-NLO will require complementary measurements or a priori knowledge of one of the parameters, these observables offer additional axes through which spatially and spectrally indistinguishable particles can be resolved. In this study, we focus on the use of the vpFT-NLO phase to achieve subdiffraction spatial resolution based on the individual polarization dependences of gold nanorods.

Super-resolution Imaging with vpFT-NLO Microscopy

To demonstrate the application of vpFT-NLO microscopy to achieving subdiffraction spatial resolution, two gold nanorods which are colocated within the optical diffraction limit of ~250 nm were studied. As shown in Figure 3a, these nanorods have

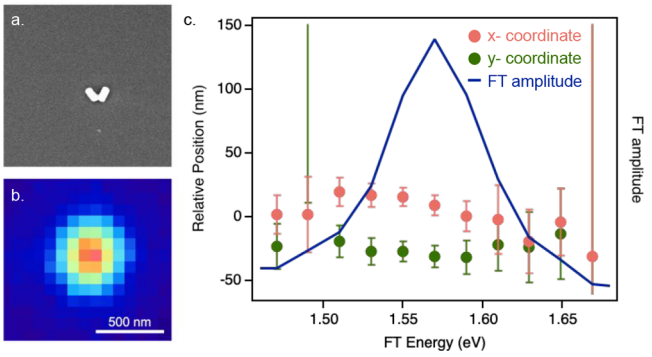

Figure 3. (a) SEM image and (b) diffraction-limited MPPL-detected optical image of two nanorods. (c) FT-NLO analysis of the same nanorod pair in (a,b) demonstrates no appreciable shift in the x (pink) and y (green) coordinates of the center of mass of the emission as a function of Fourier transform energy. The FT spectrum (blue) also exhibits only one resolvable component, precluding optical resolution of the two particles imaged in (a).

dimensions of approximately 120 × 60 nm and have centers of mass that are separated by approximately 80 nm. Upon excitation with a broadband pulse centered at 1.55 eV, which is resonant with the LSPR (Figure S1), the nanorods exhibit multiphoton photoluminescence. The diffraction-limited MPPL image is shown in Figure 3b; as expected, the two particles are indistinguishable.

The signal from the two particles is also not separable with FT-NLO microscopy, which our previous work has demonstrated can be used to localize particles with subdiffraction spatial resolution based on variations in their resonance response. In FT-NLO microscopy, a polarizer is inserted after the pulse replica generator shown in Figure 1a to generate a pair of linearly polarized pulses that share a common polarization plane. A 2D image of the nonlinear optical signal from the nanorods is collected at a series of time delays to generate an interferometric data set in which the emission intensity from each nanoparticle is modulated due to resonant excitation of its longitudinal plasmon mode. The drift-corrected data is Fourier transformed along τ to generate a 3D data set consisting of an image of the particles at each Fourier transform energy step. For particles which can be distinguished based on their resonance spectra, a shift in the center of the nonlinear emission point spread function can be observed as a function of Fourier transform energy, as in ref 24 and Figure S3.[24] To test whether FT-NLO microscopy is sufficient to separate the signal from the particles without the need for variable polarization, the center of mass of the emission was determined by fitting the image at each Fourier transform energy step with a 2D Gaussian function. The x- and y-coordinates obtained from the fitting are plotted as a function of energy in Figure 3c. For the particle pair studied in this work, no clear shift in the x (pink) or y (green) emission position with energy is observed (Figure 3c). Additionally, the Fourier transform spectrum of the particles (Figure 3c, blue line) does not exhibit obvious contributions from multiple components; the FT spectrum is accurately accounted for using a single Lorentzian function. From this, we conclude that the resonance spectra of the two particles are too similar to allow resolution of the individual particles with FT-NLO microscopy. This is supported by SEM imaging indicating that the nanorods both have aspect ratios of approximately 2, which is expected to result in similar LSPR energies.[25]

Next, we demonstrate that although the differences in the resonance energies are insufficient to distinguish the two particles using standard FT-NLO microscopy, they can be resolved in vpFT-NLO based on their polarization dependences. Removing the polarizer after the pulse replica generator creates a fundamental beam with controllably variable polarization, as shown in Figure 1. As discussed above, the phase of the Fourier transform is sensitive to the circular dichroism of the particle. The nanorods in Figure 3 were next studied with vpFT-NLO. Similarly to FT-NLO microscopy, an image of the nonlinear emission was collected at various time delays and Fourier transformed to generate a data set containing the amplitude of the Fourier transform at each pixel of the image for each energy step. However, the phase of the Fourier transform at each pixel was also retained to yield an additional dimension of information. Figure 4 shows a slice of

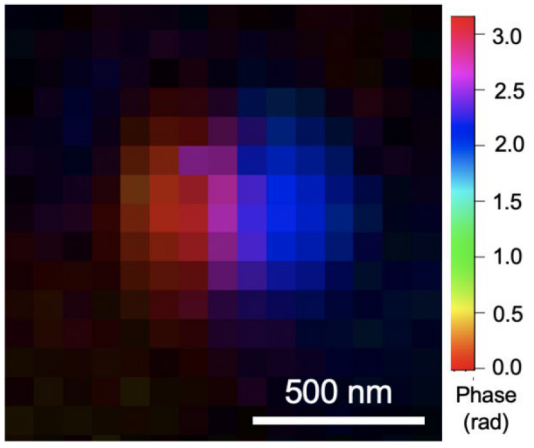

Figure 4. Analysis of the same nanorod pair in Figure 3 using vpFT-NLO microscopy at an FT energy of 1.59 eV. The brightness and hue of each pixel are determined by the magnitude and phase, respectively, from FT analysis. A gamma correction of 0.8 was applied to aid visualization.

the Fourier transform data set at an energy of 1.59 eV. Each pixel in the image is false colored to indicate the magnitude (brightness) and phase (hue) of that pixel at a specific energy in the FT spectrum. From Figure 4, it is readily apparent that two particles are present which are now distinguishable due to the phase difference of their vpFT-NLO response. As discussed in the theoretical section above, while circular dichroism is expected to cause phase shifts in the vpFT-NLO signal, the amount of phase shift is also influenced by the linear dichroism of the nanorod.

https://doi.org/10.1021/cbmi.3c00008
Chem. Biomed. Imaging 2023, 1, 91−98

In order to determine the position of each particle, a global fitting algorithm was developed to simultaneously fit the magnitude and phase data for each FT energy. A 2D Gaussian function which is independent of energy, $G_i(x,y)$, was used to approximate the spatial PSF of each particle (with index i) with fitting parameters of position, width, and diagonal correlation. The amplitude and phase of each particle at a given FT energy were additional fitting parameters, denoted as $m_i(E)$ and $\phi_i(E)$ respectively. The measured magnitude and phase at a given spatial coordinate and FT energy were then fit to

$$M(x, y, E) = \{[m_1(E)\cdot G_1(x, y)]^2 + [m_2(E)\cdot G_2(x, y)]^2 + 2m_1(E)m_2(E)G_1(x, y)G_2(x, y)\cos(\phi_1(E) - \phi_2(E))\}^{1/2} \quad (12)$$

$$Ph(x, y, E) = \phi_1(E) + \arctan2[m_2\sin(\phi_2(E) - \phi_1(E)), m_1 + m_2\cos(\phi_2(E) - \phi_1(E))] \quad (13)$$

The above equations, which assume two emitting particles, can be extended to include additional particles within a diffraction limited area. The phase at each pixel was weighted by the magnitude of the corresponding point for fitting in order to suppress the fitting of pixels without signal, which exhibit a random phase.

In order to test the robustness of the method, a half-wave plate was inserted before the sample to rotate the polarization of the fundamental with respect to the nanorod longitudinal axis. The vpFT-NLO signal from the nanorod pair was measured and analyzed at five different half-wave plate angles. The signal from two other nearby nanorods was localized by fitting with a 2D Gaussian point spread function and used to correlate the results from the vpFT-NLO analysis to the electron microscopy images (Figure 5 and Figure S4).

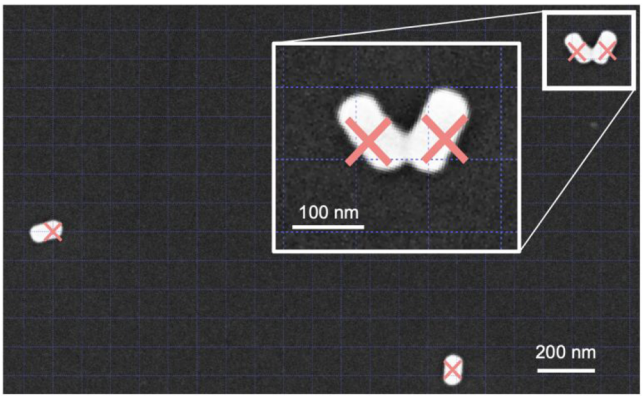

Figure 5. Comparison of nanorod positions determined optically through vpFT-NLO (pink crosses) and scanning electron microscopy.

Generally, the fitting algorithm is able to differentiate the two nanorods in the particle pair and determine their positions within ~50 nm when compared to addition characterization by electron microscopy. There is some variation in the retrieved position of the rods for different experimental trials shown in Figure S4, which may result from several factors. First, we approximate the PSF of each individual rod as a 2D Gaussian. However, the finite size of the nanorods may affect the assumption that they act as point source emitters. We also assume that the MPPL emission originates from the center of mass of the nanorod. However, previous near-field optical studies have suggested that nonlinear emission may be localized to the tips of the nanorods.[31] Finally, the two nanorods studied here are close enough that coupling may occur,[32,33] resulting in polarization-selective hybrid modes which may complicate the localization of the emission to one of the particles.

Here, we have demonstrated that the polarization resolution of the vpFT-NLO method can resolve two nanorods which were not separable spatially in a diffraction-limited measurement or based on their frequency response. The ability to resolve any two particles using vpFT-NLO will depend on their spatial separation as well as their distinction in polarization- and frequency-dependent resonance responses. The detection of higher order nonlinear optical signals may enhance the achievable resolutions through the increased intrinsic contrast between polarization states as the nonlinear order increases. The extension to other nanoparticle systems, such as coupled dimers of nanospheres, will require a consideration of how the particle size, geometry, and coupling contributes to the polarization and frequency of any hybrid modes. Large aggregates of particles will further complicate this analysis, however, vpFT-NLO may provide an avenue to study the spatial localization of hybrid modes in nanoparticle assemblies. Additionally, the analysis assumes that the particles are immobilized on a background-free substrate during the measurement. Particle movement, or the presence of scattering media in the sample may degrade the achievable resolution by decreasing or eliminating the polarization-dependent response.

The effects of circular and linear dichroism on the amplitude and phase of the vpFT-NLO interferograms discussed above may offer a route to quantifying the circular dichroism and orientation of a particle. While previous works have demonstrated the use of polarization modulation or point-spread function engineering approaches to resolve the orientation of single particles,[34−37] vpFT-NLO can be used to distinguish particles through both their polarization- and excitation-energy-dependent nonlinear optical emission. As such, vpFT-NLO uniquely simultaneously provides the highly desirable resonance response of the object.

CONCLUSIONS

We have demonstrated a Fourier-transform imaging technique based on controllable interferometric modulation of the polarization state of the excitation beam and 2D array detection of nonlinear optical signals from gold nanorods. In the vpFT-NLO data, differences in the polarization and resonance response of nano-objects are encoded in both the phase and amplitude of the optical interferograms and corresponding Fourier transform spectra. Through examination of the phase of the FT data set, particles which were not resolvable through diffraction-limited microscopy or FT-NLO are readily distinguishable in vpFT-NLO. In the gold nanorod case study presented here, nanoparticles separated by less than 50 nm were resolved, which is an approximate 5-fold improvement over expectations based on the 250 nm diffraction-limited spot size of the measurement. While the results in this study were obtained by detection of MPPL from gold nanorods, the vpFT-NLO method is generalizable to any nonlinear signal which exhibits a frequency or polarization dependence. Therefore, extension to other label-free NLO

https://doi.org/10.1021/cbmi.3c00008
Chem. Biomed. Imaging 2023, 1, 91−98

observables such as harmonic generation and nonlinear Raman signals should be possible given incorporation of the appropriate response functions. Extension to higher-order processes may allow for greater sensitivity of the measurement.

■ ASSOCIATED CONTENT

Supporting Information

The Supporting Information is available free of charge at https://pubs.acs.org/doi/10.1021/cbmi.3c00008.

Detailed experimental methods and supporting figures (PDF)

FT-NLO interferometric data set of the particle pair shown in Figure 3 (MP4)

vpFT-NLO interferometric data set of the particle pair shown in Figure 3 (MP4)

■ AUTHOR INFORMATION

Corresponding Author

Kenneth L. Knappenberger, Jr. − *Department of Chemistry, The Pennsylvania State University, University Park, Pennsylvania 16802, United States;* orcid.org/0000-0003-4123-3663; Email: klk260@psu.edu

Author

Megan A. Steves − *Department of Chemistry, The Pennsylvania State University, University Park, Pennsylvania 16802, United States;* Present Address: California Institute for Quantitative Biosciences, University of California, Berkeley, Berkeley, California 94720, United States; orcid.org/0000-0002-1410-5650

Complete contact information is available at: https://pubs.acs.org/10.1021/cbmi.3c00008

Notes

The authors declare no competing financial interest.

■ ACKNOWLEDGMENTS

This work was supported by a grant from the Air Force Office of Scientific Research (FA-22-1-0402), the National Science Foundation (award CHE-2204190) and the NSF graduate research fellowship program under award DGE1255832. The authors thank Wesley Auker for performing SEM imaging and Joseph Tracy for providing samples.

■ REFERENCES

(1) Adhikari, S.; Orrit, M. Progress and Perspectives in Single-Molecule Optical Spectroscopy. *J. Chem. Phys.* **2022**, *156* (16), 160903.

(2) Moerner, W. E. Viewpoint: Single Molecules at 31: What's Next? *Nano Lett.* **2020**, *20* (12), 8427−8429.

(3) Xiang, L.; Chen, K.; Xu, K. Single Molecules Are Your Quanta: A Bottom-Up Approach toward Multidimensional Super-Resolution Microscopy. *ACS Nano* **2021**, *15* (8), 12483−12496.

(4) Zhang, Z.; Kenny, S. J.; Hauser, M.; Li, W.; Xu, K. Ultrahigh-Throughput Single-Molecule Spectroscopy and Spectrally Resolved Super-Resolution Microscopy. *Nat. Methods* **2015**, *12* (10), 935−938.

(5) Backer, A. S.; Lee, M. Y.; Moerner, W. E. Enhanced DNA Imaging Using Super-Resolution Microscopy and Simultaneous Single-Molecule Orientation Measurements. *Optica* **2016**, *3* (6), 659−666.

(6) Ding, T.; Wu, T.; Mazidi, H.; Zhang, O.; Lew, M. D. Single-Molecule Orientation Localization Microscopy for Resolving Structural Heterogeneities between Amyloid Fibrils. *Optica* **2020**, *7* (6), 602−607.

(7) Cruz, C. A. V.; Shaban, H. A.; Kress, A.; Bertaux, N.; Monneret, S.; Mavrakis, M.; Savatier, J.; Brasselet, S. Quantitative Nanoscale Imaging of Orientational Order in Biological Filaments by Polarized Superresolution Microscopy. *Proc. Natl. Acad. Sci. U. S. A.* **2016**, *113* (7), E820−E828.

(8) Burns, D. H.; Callis, J. B.; Christian, G. D.; Davidson, E. R. Strategies for Attaining Superresolution Using Spectroscopic Data as Constraints. *Appl. Opt.* **1985**, *24*, 154.

(9) Betzig, E. Proposed Method for Molecular Optical Imaging. *Opt. Lett.* **1995**, *20*, 237.

(10) Rust, M. J.; Bates, M.; Zhuang, X. Sub-Diffraction-Limit Imaging by Stochastic Optical Reconstruction Microscopy (STORM). *Nat. Methods* **2006**, *3* (10), 793−795.

(11) Betzig, E.; Patterson, G. H.; Sougrat, R.; Lindwasser, O. W.; Olenych, S.; Bonifacino, J. S.; Davidson, M. W.; Lippincott-Schwartz, J.; Hess, H. F. Imaging Intracellular Fluorescent Proteins at Nanometer Resolution. *Science (1979)* **2006**, *313* (5793), 1642−1645.

(12) Sharonov, A.; Hochstrasser, R. M. Wide-Field Subdiffraction Imaging by Accumulated Binding of Diffusing Probes. *Proc. Natl. Acad. Sci. U. S. A.* **2006**, *103* (50), 18911−18916.

(13) Dertinger, T.; Colyer, R.; Iyer, G.; Weiss, S.; Enderlein, J. Fast, Background-Free, 3D Super-Resolution Optical Fluctuation Imaging (SOFI. *Proc. Natl. Acad. Sci. U. S. A.* **2009**, *106* (52), 22287.

(14) Zhanghao, K.; Chen, L.; Yang, X.-S.; Wang, M.-Y.; Jing, Z.-L.; Han, H.-B.; Zhang, M. Q; Jin, D.; Gao, J.-T.; Xi, P. Super-Resolution Dipole Orientation Mapping via Polarization Demodulation. *Light: Sci. Appl.* **2016**, *5* (10), e16166−e16166.

(15) Artigas, D.; Merino, D.; Polzer, C.; Loza-Alvarez, P. Sub-Diffraction Discrimination with Polarization-Resolved Two-Photon Excited Fluorescence Microscopy. *Optica* **2017**, *4* (8), 911−918.

(16) Guan, M.; Wang, M.; Zhanghao, K.; Zhang, X.; Li, M.; Liu, W.; Niu, J.; Yang, X.; Chen, L.; Jing, Z.; Zhang, M. Q.; Jin, D.; Xi, P.; Gao, J. Polarization Modulation with Optical Lock-in Detection Reveals Universal Fluorescence Anisotropy of Subcellular Structures in Live Cells. *Light: Science & Applications 2022 11:1* **2022**, *11* (1), 1−13.

(17) Chandra, M.; Dowgiallo, A. M.; Knappenberger, K. L. Magnetic Dipolar Interactions in Solid Gold Nanosphere Dimers. *J. Am. Chem. Soc.* **2012**, *134* (10), 4477−4480.

(18) Kumar Balla, N.; Rendón-Barraza, C.; Hoang, L. M.; Karpinski, P.; Bermúdez-Ureña, E.; Brasselet, S. Polarized Nonlinear Nanoscopy of Metal Nanostructures. *ACS Photonics* **2017**, *4* (2), 292−301.

(19) Spaeth, P.; Adhikari, S.; Le, L.; Jollans, T.; Pud, S.; Albrecht, W.; Bauer, T.; Caldarola, M.; Kuipers, L.; Orrit, M. Circular Dichroism Measurement of Single Metal Nanoparticles Using Photothermal Imaging. *Nano Lett.* **2019**, *19* (12), 8934−8940.

(20) Spaeth, P.; Adhikari, S.; Baaske, M. D.; Pud, S.; Ton, J.; Orrit, M. Photothermal Circular Dichroism of Single Nanoparticles Rejecting Linear Dichroism by Dual Modulation. *ACS Nano* **2021**, *15* (10), 16277−16285.

(21) Leighton, R. E.; Alperstein, A. M.; Frontiera, R. R. Label-Free Super-Resolution Imaging Techniques. *Annu. Rev. Anal. Chem.* **2022**, *15* (1), 37−55.

(22) Min, W.; Freudiger, C. W.; Lu, S.; Xie, X. S. Coherent Nonlinear Optical Imaging: Beyond Fluorescence Microscopy. *Annu Rev. Phys. Chem.* **2011**, *62*, 507−530.

(23) Zipfel, W. R.; Williams, R. M.; Webb, W. W. Nonlinear Magic: Multiphoton Microscopy in the Biosciences. *Nat. Biotechnol.* **2003**, *21* (11), 1369−1377.

(24) Steves, M. A.; Knappenberger, K. L. Achieving Sub-Diffraction Spatial Resolution Using Combined Fourier Transform Spectroscopy and Nonlinear Optical Microscopy. *J. Chem. Phys.* **2022**, *156* (2), 021101.

(25) Link, S.; El-Sayed, M. A. Spectral Properties and Relaxation Dynamics of Surface Plasmon Electronic Oscillations in Gold and Silver Nanodots and Nanorods. *J. Phys. Chem. B* **1999**, *103* (40), 8410−8426.

(26) Li, Z.; Kang, L.; Lord, R. W.; Park, K.; Gillman, A.; Vaia, R. A.; Schaak, R. E.; Werner, D. H.; Knappenberger, K. L. Plasmon-Mediated Chiroptical Second Harmonic Generation from Seemingly Achiral Gold Nanorods. *ACS Nanoscience Au* **2022**, *2* (1), 32−39.
(27) Brida, D.; Manzoni, C.; Cerullo, G. Phase-Locked Pulse Pair for Two-Dimensional Spectroscopy by a Birefringent Delay Line. *Opt. Lett.* **2012**, *37* (15), 3027−3029.
(28) Jarrett, J. W.; Liu, X.; Nealey, P. F.; Vaia, R. A.; Cerullo, G.; Knappenberger, K. L. Communication: SHG-Detected Circular Dichroism Imaging Using Orthogonal Phase-Locked Laser Pulses. *J. Chem. Phys.* **2015**, *142* (15), 151101.
(29) Savenkov, S. N.; Marienko, V. v.; Oberemok, E. A.; Sydoruk, O. Generalized Matrix Equivalence Theorem for Polarization Theory. *Phys. Rev. E* **2006**, *74* (5), 056607.
(30) Steves, M. A.; Knappenberger, K. L. Improving Spectral, Spatial, and Mechanistic Resolution Using Fourier Transform Nonlinear Optics: A Tutorial Review. *ACS Physical Chemistry Au* **2022**, DOI: 10.1021/acsphyschemau.2c00051.
(31) Imura, K.; Nagahara, T.; Okamoto, H. Plasmon Mode Imaging of Single Gold Nanorods. *J. Am. Chem. Soc.* **2004**, *126* (40), 12730−12731.
(32) Prodan, E.; Radloff, C.; Halas, N. J.; Nordlander, P. A Hybridization Model for the Plasmon Response of Complex Nanostructures. *Science (1979)* **2003**, *302* (5644), 419−422.
(33) Sönnichsen, C.; Reinhard, B. M.; Liphardt, J.; Alivisatos, A. P. A Molecular Ruler Based on Plasmon Coupling of Single Gold and Silver Nanoparticles. *Nat. Biotechnol.* **2005**, *23* (6), 741−745.
(34) Ha, T.; Enderle, T.; Chemla, D. S.; Selvin, P. R.; Weiss, S. Single Molecule Dynamics Studied by Polarization Modulation. *Phys. Rev. Lett.* **1996**, *77* (19), 3979−3982.
(35) Peterman, E. J. G.; Sosa, H.; Goldstein, L. S. B.; Moerner, W. E. Polarized Fluorescence Microscopy of Individual and Many Kinesin Motors Bound to Axonemal Microtubules. *Biophys. J.* **2001**, *81* (5), 2851−2863.
(36) Ding, T.; Lew, M. D. Single-Molecule Localization Microscopy of 3D Orientation and Anisotropic Wobble Using a Polarized Vortex Point Spread Function. *J. Phys. Chem. B* **2021**, *125* (46), 12718−12729.
(37) Monaghan, J. W.; O'Dell, Z. J.; Sridhar, S.; Paranzino, B.; Sundaresan, V.; Willets, K. A. Calcite-Assisted Localization and Kinetics (CLocK) Microscopy. *J. Phys. Chem. Lett.* **2022**, *13*, 10527−10533.